Deformation of a Droplet in an Electric Field: Nonlinear Transient Response in Perfect and Leaky Dielectric Media.

Graeme Supeene, Charles R. Koch, and Subir Bhattacharjee *

Department of Mechanical Engineering, 4-9 Mechanical Engineering Building, University of Alberta, Edmonton, AB, T6G 2G8, Canada.

Abstract

Deformation of a fluid drop, suspended in a second immiscible fluid, under the influence of an imposed electric field is a widely studied phenomenon. In this paper, the system is analyzed numerically to assess its dynamic behavior. The response of the system to a step change in the electric field is simulated for both perfect and leaky dielectric systems, exploring the influence of the fluid, interfacial, and electrical properties on the system dynamics. For the leaky dielectric case, the dynamic build up of the free charge at the interface including the effects of convection along the interface due to electrohydrodynamic circulation is investigated. The departure of the system from linear perturbation theory is explained using these dynamic simulations. The present simulations are compared with analytic solutions, as well as available experimental results, indicating that the predictions from the model are reliable even at considerably large deformations.

Key words: Droplet deformation; Electric field; Navier-Stokes equations; Finite element; Perfect dielectric; Leaky dielectric.

1 Introduction

A fluid drop suspended in another immiscible fluid will deform when subjected to an electric field. Applications of this phenomenon encompass spraying[1], aerosols, inkjet printing, coalescence of droplets for de-emulsification purposes [2–4], and electrowetting based droplet

* Tel: (780) 492 6712; Fax: (780) 492 2200; Email: Subir.B@ualberta.ca

manipulation in microfluidic systems, [5–7], to name a few. The electrical and fluid mechanical properties of the fluids determine the nature and extent of the deformation. The problem of droplet deformation under the influence of an imposed electric field has been extensively studied from different perspectives. The mathematical foundation of the subject has been rigorously established, and several aspects of the equilibrium and transient behavior of such systems have been explored.

Figure 1 schematically depicts the fundamental parameters governing the extent of droplet deformation under the influence of an electric field. As noted in the figure, the key properties dictating the nature and extent of deformation are the viscosity, dielectric permittivity, and electric conductivity of the two fluids. The interfacial tension is unique for a given fluid-fluid interface. The deformation of a drop in an electric field is characterized by a balance of interfacial, hydrodynamic, and electrical stresses at the droplet interface. The electrical stresses cause the interface to distort, while interfacial tension tends to restore the deformation. Viscous stresses and fluid pressure gradients due to the flow fields can also alter the deformation substantially. The mathematical description of this system requires simultaneous solution of the dynamic fluid mechanical equations and the equations of electrostatics.

The destabilizing electrical force at an interface between two fluids manifests itself differently depending on the fluid electrical properties. For two perfect dielectric (insulating) fluids with different dielectric permittivities, the electric field discontinuity at the interface results in a polarization stress normal to the interface. This effect in isolation can generate transient flow patterns, but it does not tend to produce shear flow or vortices, and the steady state is generally quiescent. When the fluids contain free charge, for instance, in the form of ions, the interaction of the free charge with the imposed field results in an accumulation of these charges at the interface of the two conducting fluids. This can lead to an electrical force if the ratio between the permittivities of the two fluids differs from the ratio between their conductivities. This additional force exerted by an electric field on an interface possessing free charge may act tangentially to the interface, supporting the possibility of steady-state shear or vortex flows. These mechanisms can give rise to a diverse range of deformed shapes of the droplets.

The first analytic result predicting the deformation of a drop in an electric field was derived by O'Konski and Thacher [8] for perfectly insulating (dielectric) drops in perfectly insulating media. Subsequently, Allan and Mason [9] performed a force balance over the surface of a dielectric drop in a dielectric medium. Their result was equivalent to the O'Konski and Thacher result. Using the notations of Fig. 1, the steady state deformation, d, of the droplet predicted by the O'Konski and Thacher/Allan and Mason (OTAM) expression is

$$d_\infty = \frac{R_0 \epsilon_e |\mathbf{E}_0|^2}{\gamma} \frac{9(S-1)^2}{16(S+2)^2} \tag{1}$$

where $|\mathbf{E}_0|$ is the magnitude of the electric field vector along the z coordinate, and the

parameter S ($= \epsilon_i/\epsilon_e$) represents the ratio of dielectric permittivities of the droplet and the suspending medium. The deformation parameter, d, is defined as

$$d = \frac{b-a}{b+a} \tag{2}$$

where a is the equatorial radius of the spheroid and b is the polar half-axis. The symbol d_∞ is used in Eq. (1), and in the rest of the paper to indicate that the deformation is evaluated at steady state. According to Eq. (1), the deformation must always be positive, *i.e.*, the resultant deformed shape is always a prolate spheroid, elongated in the direction of the electric field. Allan and Mason [9], however, observed discrepancies between the predictions of Eq. (1) and their experiments on electrical deformation of droplets. In some of their experiments oblate deformation (compression in the axis of the applied field) was observed, which was clearly beyond the scope of Eq. (1).

Taylor [10] and later Melcher and Taylor [11] developed an electrohydrodynamic model for the deformation of conducting droplets suspended in a conducting medium under the influence of an imposed electric field. This model, generally referred to as the "leaky dielectric model", has become a cornerstone of the theory of electrical drop deformation. The expression for the steady-state deformation in this model is

$$d_\infty = \frac{R_0\epsilon_e|\mathbf{E}_0|^2}{\gamma}\,\frac{9}{16(2+H)^2}\left[H^2+1-2S+3(H-S)\left(\frac{2+3M}{5+5M}\right)\right] \tag{3}$$

where

$$S = \frac{\epsilon_i}{\epsilon_e}, \quad H = \frac{\sigma_i}{\sigma_e}, \quad M = \frac{\mu_i}{\mu_e}$$

Equation (3) successfully predicted the oblate deformations observed in the experiments of Allan and Mason [9]. The leaky dielectric model, however, suffers the limitation that it is invalid for perfect dielectric systems. This is immediately apparent from Eq. (3), where setting $\sigma_i = \sigma_e = 0$ does not yield the OTAM expression (Eq. 1).

The leaky dielectric model has been elaborated upon in several subsequent works, notably [12–17], which specifically focus on the transport modes of the free charge carriers (ions). A comprehensive review of the theoretical developments in this area was given by Saville [15]. Zholkovskij *et al.* [16] provided a solution for the electrokinetic problem that resolved the disparity between the OTAM and Taylor results in the limit of zero conductivity. More recently, an extension of the Taylor model was proposed [17].

All the above mentioned approaches pertain to steady-state analysis of small deformations under the influence of small electric fields. These results do not apply to the dynamic problem,

and cannot address large deformations or break up of droplets. The transient electrohydrodynamic problem addressing the deformation of droplets is also an extensively studied subject [18–24].

Since the theoretical treatments of drop deformation in an electric field are limited to small deformations, or large deformations with assumptions placed on the shape, there has been a significant and continuing interest in finding numerical solutions to these problems. Numerical solutions do not suffer from the same limitations as the analytic theories, although care must be taken to ensure the correctness of the results. Attempts to model this problem computationally appear quite early following the initial analytic efforts.

The pioneering computational studies on transient deformation of droplets appeared in the early 1970s [25,26]. These studies deal with conducting drops with constant surface potential, both isolated and in pairs, and with isolated charged drops. A finite perturbation technique was employed to converge to the correct force balance for this system, yielding the steady-state result, which for relatively large deformations showed a small deviation from the spheroidal shape. The irrotational, inviscid fluid mechanics equations were solved to provide dynamic analyses of drop deformation and contact between drop pairs. The simulations with individual drops showed the development of conical tips in extreme cases of deformation.

The steady-state perfect dielectric problem was solved using Newton's method with stepwise changes in applied field [27]. Sherwood [13] analyzed the leaky dielectric model by means of a boundary integral method. Viscosity was included in the model, but the droplet and medium were assumed to be equally viscous. The momentum term in the Navier-Stokes equations was neglected, as the boundary integral method is not capable of dealing with nonlinearity. Large deformations were obtained by stepwise increases in the applied field. Sherwood's results indicate that when the permittivity ratio ϵ_i/ϵ_e is sufficiently high, the drop develops the pointed ends characteristic of tip streaming, whereas a high conductivity ratio tends to produce the bulbous-ended breakup mode.

Finite element analysis of the shape patterns and stability of a charged drop in an electric field was conducted by Basaran and Scriven [28,29]. Their steady-state analysis assumed infinite drop conductivity, so that the final state did not involve flow, and hence the fluid mechanics equations were not necessary. Haywood *et al.* [30] developed a numerical technique to predict the transient deformation of a perfect dielectric system. Differences between the stability limits predicted from steady-state analysis and from their fully dynamic model were observed. Tsukada *et al.* [31] performed finite element calculations using Taylor's leaky dielectric model and compared their numerical results with experiments. These numerical results showed a substantial improvement in predictive power over the analytic formulae. Feng and Scott [22] employed the Galerkin finite element technique in a comprehensive steady-state analysis of the leaky dielectric model. The effect of charge convection was also treated [24] where a parameter called electric Reynolds number was introduced. This is a ratio of the time scales of charge convection and conduction, and if it is nonzero, the final

interfacial charge distribution and droplet deformation can be altered significantly.

The method of Tsukada *et al.* [31] was extended to deal with the full dynamic problem of a leaky dielectric droplet subjected to a step jump in applied field of arbitrary magnitude [32]. The dynamic response of their model was compared with a highly oscillatory solution obtained in an earlier work [33], in which pure droplet oscillations were studied in absence of electric fields. Excellent agreement was observed in the predictions from the two approaches. Charge convection and finite conduction times were not considered.

In this paper we present a numerical scheme based on the finite element method incorporating a moving boundary implementation for simulation of the transient deformation of a droplet in an electric field. The method is capable of simulating perfect dielectric fluids or fluids with finite conductivity, as long as the charge buildup occurs in a layer much smaller in thickness compared to the droplet radius. The time dependence of the electrical conduction can also be taken into account, along with finite charge convection effects on the drop interface. Large deformations are simulated up to the point of droplet disintegration in some cases. The steady-state deformations are compared against Eqs. (1) and (3) for the perfect and leaky dielectric systems, respectively, under small deformations, and deviations from these limiting cases at higher imposed fields have been studied. The transient deformation behavior when the charge buildup dynamics is explicitly incorporated in the model is also explored. Finally, a comparison with experimental results of deformation available in literature has been presented.

2 Theory

In this section, we will first present the general governing equations for the droplet deformation under the influence of an electric field. Following this, the simplified transient equations for the perfect dielectric and the leaky dielectric cases will be presented. In most parts, the general formulation is based on the approaches detailed elsewhere [15,34].

2.1 General Electrokinetic Model

Referring to Fig. 1, we will consider two sets of governing equations pertaining to the droplet and the suspending fluid phases. The governing equations for each phase are the Navier-Stokes equation (modified by including the electrical body force), the Poisson equation, and the Nernst-Planck equations describing the transport of the free charge carriers.

The fluid flow in the system will be governed by the Navier-Stokes equation

$$\rho_{i,e}\frac{\partial \mathbf{u}_{i,e}}{\partial t} + \rho_{i,e}\mathbf{u}_{i,e}\cdot\nabla\mathbf{u}_{i,e} = -\nabla p_{i,e} + \nabla\cdot\mu_{i,e}\left(\nabla\mathbf{u}_{i,e} + \nabla\mathbf{u}_{i,e}^{T}\right) + \rho_{i,e}^{f}\mathbf{E}_{i,e} \tag{4}$$

along with the continuity equation

$$\nabla\cdot\mathbf{u}_{i,e} = 0 \tag{5}$$

In writing these equations, we have neglected the effect of gravity, included an electric body force, $\rho^f\mathbf{E}$, where ρ^f is the volumetric free charge density, and assumed incompressible fluids. The subscripts i and e correspond to the droplet and the suspending medium, respectively. $\mathbf{u}$ is the fluid velocity vector and p is the pressure. Neglecting gravity makes consideration of density differences irrelevant, and hence, in subsequent discussion, we will assume both fluids to have the same density.

The electric field distribution, $\mathbf{E} = -\nabla\psi$, is governed by the potential (ψ) distribution according to the Poisson equation

$$\nabla\cdot\epsilon_{i,e}\nabla\psi_{i,e} = -\rho_{i,e}^{f} \tag{6}$$

where the volumetric free charge density is

$$\rho_{i,e}^{f} = \sum_{k=1}^{n} z^k e n_{i,e}^{k} \tag{7}$$

with k representing the k^{th} ionic species.

The ionic fluxes, $\mathbf{j}^k$, are governed by the Nernst-Planck equations

$$\mathbf{j}_{i,e}^{k} = n_{i,e}^{k}\mathbf{u}_{i,e} - D_{i,e}^{k}\nabla n_{i,e}^{k} - \frac{z^k e n_{i,e}^{k} D_{i,e}^{k}}{k_B T}\nabla\psi_{i,e} \tag{8}$$

Here, n^k denotes the number concentration of the k^{th} ionic species. The Nernst-Planck equation describes the ion transport due to convection, diffusion and electro-migration. The ionic fluxes appear in the ionic species conservation equations, written as

$$\frac{\partial n_{i,e}^{k}}{\partial t} = -\nabla\cdot\mathbf{j}_{i,e}^{k} \tag{9}$$

While Eqs. (4) to (9) constitute the fundamental governing equations for the electrohydrodynamic problem in each fluid phase, certain additional conditions apply to these systems, which are related to the electric current. The current density in the system is given by

$$\mathbf{i}_{i,e} = e\sum_{k=1}^{n} z^k \mathbf{j}_{i,e}^k \tag{10}$$

After substituting Eq. (8) in (10), one obtains

$$\mathbf{i}_{i,e} = e\mathbf{u}_{i,e}\sum z^k n_{i,e}^k - e\sum D_{i,e}^k z^k \nabla n_{i,e}^k - \sigma_{i,e}\nabla\psi_{i,e} \tag{11}$$

where

$$\sigma_{i,e} = \frac{e^2}{k_B T}\sum (z^k)^2 D_{i,e}^k n_{i,e}^k \tag{12}$$

is the solution conductivity. Note that in a homogeneous electroneutral liquid phase, Eq. (11) yields Ohm's law, $\mathbf{i} = -\sigma\nabla\psi$.

Applying conservation of charge principle, one can multiply Eq. (9) by $z^k e$ and sum over all ionic species to write

$$e\frac{\partial}{\partial t}\sum z^k n_{i,e}^k = -e\nabla\cdot\sum z^k \mathbf{j}_{i,e}^k = -\nabla\cdot\mathbf{i}_{i,e} \tag{13}$$

in which, the final term on the right hand side utilizes Eq. (10). Noting that the term $e\sum z^k n^k$ on the left hand side of Eq. (13) represents the volumetric free charge density, ρ^f, one can use Poisson's equation, (6), to write

$$\nabla\cdot\left[\frac{\partial}{\partial t}(\epsilon_{i,e}\nabla\psi_{i,e})\right] = \nabla\cdot\mathbf{i}_{i,e} \tag{14}$$

Utilizing $\mathbf{E} = -\nabla\psi$, one can simplify the above equation to

$$\nabla\cdot\left[\frac{\partial(\epsilon_{i,e}\mathbf{E}_{i,e})}{\partial t} + \mathbf{i}_{i,e}\right] = 0 \tag{15}$$

which is the generalized statement for the continuity of current in each phase. At steady state, the displacement current (first term) vanishes from Eq. (15), yielding $\nabla\cdot\mathbf{i}_{i,e} = 0$.

These equations apply to the two phases (droplet and the suspending medium) independently. Two of the primary variables of the governing equations are strictly continuous at

the droplet-suspending medium interface. These include the fluid velocity and the electric potential. The current is also continuous across the interface. The ion concentrations and pressure are, however, discontinuous at the interface.

The overall force balance at the interface can be written by considering the viscous, electrical (Maxwell), and the interfacial stresses. This relationship takes the form of an interfacial boundary condition at the droplet surface. The net stress vector at the interface is given by

$$\begin{aligned}\overline{\overline{T}}\cdot\mathbf{n} = &-\left[-p_i\,\overline{\overline{I}}+\mu_i(\nabla\mathbf{u}_i+\nabla\mathbf{u}_i^T)\right]\cdot\mathbf{n}+\left[-p_e\,\overline{\overline{I}}+\mu_e[\nabla\mathbf{u}_e+\nabla\mathbf{u}_e^T)\right]\cdot\mathbf{n}\\ &-\left[\epsilon_i\mathbf{E}_i\mathbf{E}_i-\frac{1}{2}\epsilon_i\mathbf{E}_i\cdot\mathbf{E}_i\,\overline{\overline{I}}\right]\cdot\mathbf{n}+\left[\epsilon_e\mathbf{E}_e\mathbf{E}_e-\frac{1}{2}\epsilon_e\mathbf{E}_e\cdot\mathbf{E}_e\,\overline{\overline{I}}\right]\cdot\mathbf{n}\\ &-2\gamma X\,\overline{\overline{I}}\cdot\mathbf{n}\end{aligned}\tag{16}$$

Here, $\mathbf{n}$ is the unit outward normal to the drop surface, $\overline{\overline{I}}$ is the unit tensor, γ is the interfacial tension, and X is the mean curvature of the interface, with the convention that the curvature is positive for a convex surface. Equation (16) indicates that in absence of electrical and hydrodynamic stresses, absence of any net stress at the interface would require $p_i - p_e = 2\gamma X$. When an electric field is applied to the drop, this equilibrium is disturbed, with the electrical stresses creating an imbalance in the fluid stress. This drives the fluid flow, which deforms the interface and eventually, the interface shape readjusts to establish a new equilibrium shape.

Other boundary conditions for the problem are relatively straightforward, and will be discussed later in context of the perfect and leaky dielectric representations.

An additional relationship between the individual ionic species concentrations in the two phases must be provided to solve these equations. This is problematic, since an unequivocal closure cannot be obtained unless the detailed chemistry of the system is invoked. Considering the state of the system before application of an external electric field, one might assume that the individual ionic species are equilibrium partitioned between the two phases, with a partition coefficient defined by

$$\Phi_k = \frac{n_i^k}{n_e^k}\tag{17}$$

While this definition seems adequate, it raises a few concerns about the electrical properties of the system. If the partition coefficient of different ions are different, then the droplet and the surrounding fluid will acquire equal and opposite charges. What happens to such a system when an external electric field is imposed becomes a challenging question. Certainly, the possibility of electrophoretic movement of the drop cannot be ruled out under such circumstances. Secondly, if the droplet surface is charged (due to presence of free charges

at the interface) before addition of electrolyte, the ensuing accumulation of counterions can alter the partitioning process. Finally, partition coefficient is an equilibrium thermodynamic concept, which is definitely affected under dynamic situations.

Several other issues crop up when defining the problem at the complete electrokinetic resolution. The key issues are related to the definitions of electrostatic boundary conditions at the droplet surface. As stated earlier, a complete picture is not attainable unless the detailed chemistry of the system is invoked. These problems have often led to attempts of simplifying the governing equations by making suitable assumptions about the system. A simple assumption pertains to the case when both the fluids are perfect dielectrics, which leads to the perfect dielectric (OTAM) model. The second assumption relates to a system where at least one, or both of the phases (droplet and suspending fluid) are conducting, leading to the so-called leaky-dielectric (Taylor) model. We now describe the simplified equations dealt with in these two models.

2.2 Perfect Dielectric Model

When we consider two perfect dielectric liquids, the governing equations for electrostatics simplify to the Laplace equation for both phases

$$\nabla \cdot \epsilon_{i,e} \nabla \psi_{i,e} = 0 \tag{18}$$

Since there is no free charge in the fluids, the electric body force term vanishes from the Navier-Stokes equation, leading to

$$\rho_{i,e} \frac{\partial \mathbf{u}_{i,e}}{\partial t} + \rho_{i,e} \mathbf{u}_{i,e} \cdot \nabla \mathbf{u}_{i,e} = -\nabla p_{i,e} + \nabla \cdot \mu_{i,e} \left(\nabla \mathbf{u}_{i,e} + \nabla \mathbf{u}_{i,e}^T \right) \tag{19}$$

The interfacial stress condition, Eq. (16), simplifies in this case, since both the fluid and electrostatic stresses will only act normal to the interface. Thus, the component $\overline{\overline{T}} \cdot \mathbf{n} \cdot \mathbf{n}$ becomes

$$\begin{aligned} \overline{\overline{T}} \cdot \mathbf{n} \cdot \mathbf{n} = & (p_i - p_e) + \frac{1}{2}(\epsilon_i |\mathbf{E}_i|^2 - \epsilon_e |\mathbf{E}_e|^2) \\ & + \left[\mu_e (\nabla \mathbf{u}_e + \nabla \mathbf{u}_e^T) \cdot \mathbf{n} - \mu_i (\nabla \mathbf{u}_i + \nabla \mathbf{u}_i^T) \cdot \mathbf{n} \right] \cdot \mathbf{n} \\ & + (\epsilon_e \mathbf{E}_e \mathbf{E}_e \cdot \mathbf{n} - \epsilon_i \mathbf{E}_i \mathbf{E}_i \cdot \mathbf{n}) \cdot \mathbf{n} - 2\gamma X \end{aligned} \tag{20}$$

while the tangential stress components, $\overline{\overline{T}} \cdot \mathbf{n} \cdot \mathbf{t}_j$ vanish. Here, $\mathbf{t}_j$ $(j = 1, 2)$ represent the unit vectors along the two orthogonal coordinates tangential to the surface of the drop.

The boundary conditions for the electrostatic problem are as follows:

$$\nabla\psi_e = -\mathbf{E}_0 \qquad \text{at infinity} \tag{21a}$$
$$\psi_i = \psi_e \qquad \text{at interface} \tag{21b}$$
$$\epsilon_i \mathbf{E}_i \cdot \mathbf{n}_i + \epsilon_e \mathbf{E}_e \cdot \mathbf{n}_e = 0 \qquad \text{at interface} \tag{21c}$$

Equation (21a) represents the application of a defined uniform electric field $\mathbf{E}_0$ far from the drop. Equations (21b) and (21c) represent continuity of electric potential and displacement at the interface, respectively. The displacement is continuous when the interface contains no free charge. Note that $\mathbf{n}_i = -\mathbf{n}$ where $\mathbf{n}$ is the unit outward normal to the drop surface.

At steady-state, the normal interfacial stress across the deformed droplet will vanish. This implies that the normal interfacial stress condition, Eq. (20), with $\overline{\overline{T}} \cdot \mathbf{n} \cdot \mathbf{n} = 0$ constitutes one boundary condition for the fluid mechanics problem at the droplet surface. The other two boundary conditions for the Navier-Stokes equation are:

$$-p_e \,\overline{\overline{I}} + \mu_e(\nabla \mathbf{u}_e + \nabla \mathbf{u}_e^T) = \overline{\overline{0}} \qquad \text{at infinity} \tag{22a}$$
$$\mathbf{u}_i = \mathbf{u}_e \qquad \text{at interface} \tag{22b}$$

2.3 Leaky Dielectric Model

In the case of Taylor's leaky dielectric model [11], ion diffusion is ignored, and the electric double layer is assumed to be of infinitesimal thickness and confined to the droplet-suspending fluid interface. This reduces the net free charge to a boundary condition, and once again, the ionic free charge density, ρ^f, is zero in the bulk fluid phases.

There are two ways in which the charge transport may be described. First, if the boundary charge is assumed to be in static equilibrium, the Laplace equation may be written for each of the bulk phases in accordance with the principle of continuity of current, Eq. (15), as follows:

$$\nabla \cdot \mathbf{i}_{i,e} = \nabla \cdot [-\sigma_{i,e} \nabla \psi_{i,e}] = 0 \tag{23}$$

Here $\sigma_{i,e}$ denotes the local conductivity of the fluid, which is uniform in each phase. The Navier-Stokes equation in this case assumes the same form as in Eq. (19) in each phase.

The formulation of Laplace equation in Eq. (23) allows a natural interfacial boundary description for the electrostatic equation, in which the continuity of current across the interface

is described by the use of a Neumann continuity condition

$$\sum_{j=i,e} [\nabla(\sigma_j \psi_j) \cdot \mathbf{n}_j] = 0 \tag{24}$$

The mathematical formulation employing the above expression will be referred to as the static boundary leaky-dielectric model.

A more general form is an explicit treatment, where conduction and convection of charge carriers are modelled directly. For simplicity, following Zholkovskij *et al.* [16], it is assumed that no solute adsorbs on the interface, so that the ion layer is due to electrical effects. Since the surface charge density q represents a discontinuity in electric displacement, the corresponding boundary condition can be written as

$$\sum_{j=i,e} [\nabla(\epsilon_j \Psi_j) \cdot \mathbf{n}_j] = q \tag{25}$$

If convection/diffusion are taken into account, or if the time scale of charge migration is important, an extra equation to describe the dynamics of charge transport to and from the boundary needs to be provided. Saville [15] gives the expression

$$\frac{\partial q}{\partial t} + \mathbf{u} \cdot \nabla_s q = q\mathbf{n} \cdot (\mathbf{n} \cdot \nabla)\mathbf{u} - ||\sigma \mathbf{E}|| \cdot \mathbf{n} \tag{26}$$

where the use of $||\cdots||$ indicates the jump from inside to outside, $\mathbf{n}$ is the outward normal in that direction, and ∇_s is the tangential or surface gradient. The second term on the left is the convective flux along the boundary, and the first term on the right is the change in concentration due to dilation of the interface; this can be seen by considering the incompressibility condition. The term on the far right is the current discontinuity, or charge buildup due to migration.

The fluid dynamic boundary conditions, Eqs. (22a) and (22b), also apply for the leaky dielectric case. The interfacial stress condition, however, requires an additional tangential stress arising from the interfacial charge. The conditions that the normal and tangential interfacial stresses vanish at steady state are explicitly given by

$$\begin{aligned} \bar{\bar{T}} \cdot \mathbf{n} \cdot \mathbf{n} = & (p_i - p_e) + \frac{1}{2}(\epsilon_i |\mathbf{E}_i|^2 - \epsilon_e |\mathbf{E}_e|^2) \\ & + \left[\mu_e(\nabla \mathbf{u}_e + \nabla \mathbf{u}_e^T) \cdot \mathbf{n} - \mu_i(\nabla \mathbf{u}_i + \nabla \mathbf{u}_i^T) \cdot \mathbf{n}\right] \cdot \mathbf{n} \\ & + (\epsilon_e \mathbf{E}_e \mathbf{E}_e \cdot \mathbf{n} - \epsilon_i \mathbf{E}_i \mathbf{E}_i \cdot \mathbf{n}) \cdot \mathbf{n} - 2\gamma X = 0 \end{aligned} \tag{27}$$

and

$$\bar{\bar{T}} \cdot \mathbf{n} \cdot \mathbf{t}_j = \Big[\mu_e(\nabla \mathbf{u}_e + \nabla \mathbf{u}_e^T) \cdot \mathbf{n} - \mu_i(\nabla \mathbf{u}_i + \nabla \mathbf{u}_i^T) \cdot \mathbf{n}\Big] \cdot \mathbf{t}_j + (\epsilon_e \mathbf{E}_e \mathbf{E}_e \cdot \mathbf{n} - \epsilon_i \mathbf{E}_i \mathbf{E}_i \cdot \mathbf{n}) \cdot \mathbf{t}_j = 0 \tag{28}$$

Here, $\mathbf{t}_j$ is the tangential unit vector. Since the problem form employed in this paper is axisymmetric, the only relevant tangential vector is the one in the r-z plane, so this expression reduces to a single equation.

2.4 Initial Conditions

The present problem pertains to the evaluation of the transient deformation of an initially spherical droplet of radius R_0 in response to a step change in the electric field. Prior to the application of a field, $\mathbf{E}_0$ at $t = 0$, it is assumed that no electric field is present. In all cases, the system is assumed to be stationary and locally electroneutral at $t = 0$. The resulting initial conditions are expressed as follows

$$\mathbf{u} = 0 \quad \text{and} \quad p = 0 \quad \text{in suspending medium} \tag{29a}$$

$$\mathbf{u} = 0 \quad \text{and} \quad p = \frac{2\gamma}{R_0} \quad \text{in droplet} \tag{29b}$$

$$q = 0 \quad \text{on interface} \tag{29c}$$

where γ is the interfacial tension.

Equations (29a) and (29b) specify fluid quiescence over the entire domain. It is not necessary to specify an initial condition for the electric field, since the Laplace equation is static. However, in the leaky dielectric case, local electroneutrality must be enforced at $t = 0$, and Eq. (29c) corresponds to this condition.

3 Numerical Solution

The solution of the coupled system of equations presented in Section 2 yields a time-domain solution for the deformation of a perfect or leaky dielectric fluid droplet in an immiscible perfect or leaky dielectric medium. It is subject to the assumption that the electrical relaxation of the system is much faster than the fluid relaxation, and also that the interfacial tension is uniform and constant. For the leaky dielectric model to be valid, the electrostatic double layer thickness is infinitesimal compared to the droplet radius.

3.1 Computational Domain

Figure 2(a) shows the geometry used in the numerical solution. An axi-symmetric cylindrical coordinate system was used. The deforming droplet system in Figure 1 was assumed to be symmetric with respect to the polar axis of the droplet, parallel to the electric field. In the present work, it is further assumed that the fluid mechanics obeys symmetry across the equatorial plane of the droplet, and that the electrical problem follows a form of antisymmetry whereby opposite charges fulfill the same roles on opposite sides of the equator. This allows the problem domain to be further reduced, so that modeling takes place on only one quadrant of the droplet, and eliminates the possibility of drifting of the droplet's center of mass.

Meshing of the computational domain was performed using a Delaunay triangulation algorithm [35], which generates an unstructured triangular mesh on the 2D problem domain. Quadratic Lagrange elements were used for the calculation of all variables, except pressure, which was approximated employing linear triangular elements. Figure 2(b) shows the mesh, with an inset detailing the refinement at the droplet surface. The number of elements in this problem is approximately 2000, due mostly to this interfacial refinement. Both the electrostatics problem and the fluid mechanics problem use the same geometry and mesh.

3.2 Scaling Variables for the Governing Equations

Electric field, potential, and charge were scaled with respect to the applied field, $\mathbf{E}_0$, $R_0\mathbf{E}_0$, and $\epsilon_0\mathbf{E}_0$, respectively, where R_0 is the initial spherical droplet radius, and ϵ_0 is the permittivity of vacuum. Length was scaled with respect to R_0, time with respect to the characteristic timescale for oscillation of an inviscid droplet, given by [36]

$$\tau = \sqrt{\frac{(2\rho_e + 3\rho_i)R_0^3}{24\gamma}} \tag{30}$$

and pressure was scaled with respect to the Maxwell stress at a planar interface separating the two fluids under consideration

$$p_0 = |\mathbf{E}_0|^2 \left(\epsilon_e - \frac{\epsilon_e^2}{\epsilon_i}\right) \tag{31}$$

Finally, the velocity was scaled using

$$v_0 = \frac{2R_0 d_\infty}{\tau} \tag{32}$$

where d_∞ is the final steady state deformation predicted by an appropriate analytic expression such as Eq. (1) or (3). It should be noted that this characteristic velocity is simply chosen for convenience, and does not influence the numerical solution at large deformations, where the analytic expressions (1) or (3) may not be valid themselves. The above scalings lead to the definitions of the Reynolds, Rouark, and Strouhal numbers as, respectively,

$$Re = \frac{\rho v_0 R_0}{\mu}, \quad Q = \frac{\rho v_0^2}{p_0}, \quad \text{and} \quad St = \frac{\tau v_0}{R_0} \tag{33}$$

In the above, the density and viscosity assume the values corresponding to the medium (droplet or surrounding fluid) in which the parameters are evaluated.

3.3 Dynamic Solution Structure

The non-dimensionalized governing equations were solved in a sequential manner for the above geometry and initial mesh. Further details of the non-dimensionalization and mathematical formulation are available elsewhere [37]. Here we briefly describe the solution methodology. The finite element model was solved using a fixed time step with a moving mesh. The method is multistage, and electrostatics is solved separately. Figure 3 details the steps involved in the method. Parameter initialization is performed at the beginning of the simulation. During the first time step, the geometry in Figure 2 is used. For subsequent steps, the convected geometry from the previous step is used.

After defining the geometry at a given time step, the Navier-Stokes problem is defined. At this stage, in the first time step, the mesh is generated, and in subsequent steps the convected mesh from the previous step is analyzed and replaced if necessary. The Navier-Stokes setup includes equations and boundary conditions, as well as initial conditions for the first time step. In subsequent steps, the initial condition is derived from the solution at the end of the previous step. In order to allow a pressure discontinuity at the interface, separate Navier-Stokes problems are defined in the droplet and continuous phase, and continuity is maintained by coupling at the droplet surface boundary.

To complete the fluid mechanics problem, it is necessary to solve the interfacial stress condition. The boundary stress calculator obtains the interfacial tension stress, and solves the electrostatics problem using a static linear finite element solution. It then combines the interfacial tension stress with the electrical stress to produce a usable boundary condition.

Once the interfacial stress calculation is completed, the initial conditions for the solution are defined. For the first time step, they are calculated from the initial conditions specified during the Navier-Stokes setup phase. In subsequent steps, the initial conditions are generated from the previous step's solution by interpolation. Since the full Eulerian Navier-Stokes equations

are used to describe the fluid mechanics, simply moving the solution with the nodes is inadmissible because it would introduce spurious convection. Re-initialization is therefore done in place, obtaining the solution from an unmoved copy of the finite element structure and interpolating it onto the new nodes.

Solution of the fluid mechanics problem over one time step is done by using a nonlinear time-dependent solver DASPK [38]. Since DASPK uses its own timestepping scheme to produce a high-order result, a midpoint solution is employed to allow second-order convection of the geometry. This permits larger time steps than would be possible with a zero- or first-order convection scheme. DASPK takes several small backward Euler steps at the beginning of its run in order to obtain a consistent initial condition [39]. This provides smoothing of any artifacts that may be present after the previous time step's solution is mapped to the new geometry.

After the solution, the complete finite element data structure is copied into two reference structures for mesh moving and re-initialization purposes. The mesh in one of the reference structures is moved based on the average velocity over the time step, according to the method in Section 3.4. The other reference structure is left intact, and is used for re-initialization of the solution. During the rest of the postprocessing phase, the drop volume is checked, the deformation parameter is calculated, and important variables such as the deformation parameter are added to master data lists. The global simulation time is then incremented, and the entire calculation repeated over the next time step. The iterations are continued until the global time reaches a preset stop point.

The entire algorithm was implemented in Matlab, with calls made to the subroutines from the finite element package Femlab 2.3 (Comsol AB) for mesh generation, finite element data structure generation, and certain postprocessing operations. Solution of the matrix equations, and the numerical solution in the time domain were conducted by calling the appropriate solver routines (such as DASPK) directly from Matlab. Sections of the code, such as the interfacial stress calculation, solution of the interfacial boundary condition, and movement of the mesh at successive time steps were coded in Matlab.

3.4 Moving Mesh

Since the deformation of the droplet is the parameter under study, it is necessary to formulate a moving-boundary problem. The method used is a Lagrangian moving mesh, where at the end of each time step (Δt), the mesh is convected according to the local velocity. The distance moved by each mesh point, denoted by the vector $\mathbf{x}(t + \Delta t) - \mathbf{x}(t)$, where $\mathbf{x}$ is the position vector of a node, is calculated approximately using a quadratic averaging technique, taking

output times at the beginning (t), middle ($t + \Delta t/2$), and end ($t + \Delta t$) of the time step:

$$\mathbf{x}(t + \Delta t) = \mathbf{x}(t) + \Delta t \left[\frac{1}{6}\mathbf{u}(t) + \frac{2}{3}\mathbf{u}(t + \frac{\Delta t}{2}) + \frac{1}{6}\mathbf{u}(t + \Delta t) \right] \tag{34}$$

Second-order averaging is possible because the fluid mechanics time step is handled by a nonlinear solver that produces intermediate output, thus making a midpoint solution available. Since the finite elements deform as the fluid moves, they can become unacceptably strained during large deformations. To minimize numerical errors, the code checks the minimum element quality before each time step, and re-meshes the geometry if this value is too low.

3.5 Convergence Testing

The convergence of the transient solution to a correct steady-state can be tested by comparing against the steady-state analytical results for small deformation for both perfect and leaky dielectric cases. The results presented here are representative and limited to a single physical case, which will henceforth be called the base case. It approximates a water droplet in oil with a radius of 1 μm, subject to a 1 MV/m applied electric field. Deformation in the base case is small; the perfect dielectric result predicts a steady-state deformation parameter of 3.9926×10^{-4}, *cf.* Eq. (1). Table 1 details the base case parameters for perfect dielectric fluids.

Figure 4 shows the effect of altering the boundary refinement at the droplet surface across a range of values. The parameter H_{max} is a mesh size specification in the code, which indicates the spacing between the successive nodes along the specified edge of the geometry. Here it is used on the interfacial boundary, with the bulk fluid and all other boundaries left at the default resolution. The electrostatics problem is solved on the same mesh as the fluid mechanics. It was noted during testing that refinements further away from the interface have no appreciable effect on the fluid mechanics solution.

With 9 nodes on the interface ($H_{max} = 0.2$), the error in the solution is significant, though not large. Increasing the resolution to 17 nodes ($H_{max} = 0.1$) results in a reversal of the error, which suggests that multiple factors, such as error in the electrostatics solution, are contributing to the error in the first case. This implies that, despite the moderately low error, the results in general are not trustworthy at such low interfacial resolutions. At a resolution of 33 nodes on the boundary ($H_{max} = 0.05$), the results are effectively converged. The steady-state is approximately 0.02% greater than the analytic perfect dielectric result (Eq. 1). The 54-node case ($H_{max} = 0.03$) is virtually indistinguishable from the 33-node case. The global mesh in the case of the 33-node boundary contains 1424 elements, and in the case of the 54-node boundary, the global mesh contains 1960 elements. For optimum computation, the

base case is best solved with an H_{max} of 0.05, or 33 interface nodes. Simulations of larger deformations displaying nonlinearity or instability sometimes require an interface mesh size of 0.03 (54 nodes), but refinement beyond 54 nodes has little effect on the solution for parameter ranges explored in this study.

It is critical that the electrostatics solution be accurate at the interface, since the interfacial electric field drives the fluid mechanics problem. It was observed that the Maxwell stresses were most accurate when the mesh used for solving the fluid mechanics problem was used when solving the electrostatic problem.

Figure 5 shows the effect of scaled time step on the convergence of the base case perfect dielectric problem. Time was scaled in the problem employing the characteristic time for oscillation of an inviscid droplet, Eq. (30) [36]. The time step is expressed in radians, where 2π radians signifies one complete cycle of oscillation of the drop as predicted by inviscid theory. Three time steps were tested: 0.06, 0.12, and 0.15 radians. The first two cases demonstrate good agreement with one another, with a peak value difference of less than 1%. The 0.15 radian time step, on the other hand, is too large to maintain stability, and the pole of the drop oscillates in an unsteady fashion, eventually compromising the geometric integrity of the mesh.

4 Perfect Dielectric Model

A parametric study of the perfect dielectric response to small applied fields leading to relatively small droplet deformations was presented in an earlier work [40], and hence, the focus of this section will be to present representative results from simulations under high applied fields, eventually leading to destabilization and breakup of the drop. The physical parameters are as listed in Table 1, and the electric field is varied.

Figure 6 shows four results for the perfect dielectric case. The deformation parameter, d, in the vertical axis is normalized by the analytically predicted steady-state deformation, d_∞, given by Eq. (1), so that ideally each numerically obtained dynamic response should converge to 1 at large times. It is evident that for the lower two values of the electric field, the numerical result does converge almost exactly to the analytic result. The 3 MV/m case is slightly offset, which indicates the onset of nonlinearity - the droplet becomes nonspherical and the assumption of infinitesimal deformation embedded in the analytical expression begins to fail. The deformation parameter in this case is approximately 0.0036, which is relatively small. The 10 MV/m case with $d_\infty = 0.04$ is significantly nonlinear, and illustrates well the characteristic increase in elongation other researchers have observed in large prolate deformations [27,41].

Figure 7(a) shows the dynamic response for fields ranging from the base value of 1 MV/m to

a maximum value of 20 MV/m. All other parameters are those of the base case in Table 1. The equilibrium shape of the droplet corresponding to 10 MV/m applied field, and the final snapshot of the deformed droplet under an applied field of 20 MV/m are shown in Figure 7 (b) and (c), respectively. Increasing the field past 10 MV/m in the base case results in substantial nonlinearity. The electrical stress is proportional to the square of the local field, so deformation increases rapidly with applied field. In particular, the deformation in the 20 MV/m case appears to have no steady-state value; it develops pointed tips as shown in Figure 7 (c), and the numerical method breaks down due to a singularity in the boundary curvature description. This occurs at a deformation parameter of 0.593, corresponding to an aspect ratio of 3.91. In physical systems, the development of the pointed tip precedes the emission of fluid strands and/or satellite droplets from the pole of the main droplet [9,23]. This phenomenon is known as tip streaming, and occurs when the drop permittivity is large relative to the continuous phase [13,41,42].

It may be observed from the transient behavior of the deformation that the oscillations in the dynamic response become damped as the deformation increases. At large applied fields, the deformation of the droplet appears to be almost monotonic. This may be attributed to the nonlinearity such that the electrical forcing increases with the elongation of the droplet. The initial stages of the deformation follow similar dynamics under all applied fields. As the deformation increases, the electric forcing increases, while the viscous damping and the interfacial tension (and local curvature) based restoring forces tend to decelerate the deformation. When the destabilizing electrical forces are substantially larger than the restoring forces and the viscous damping, the droplet continues a monotonic acceleration toward breakup as shown for the 20 MV/m case.

5 Leaky Dielectric Model

The leaky dielectric case in general is characterized by tangential electrical stresses on the drop surface, resulting in steady-state flow along the interface and persistent circulatory flow patterns inside the droplet. For small deformations, the static-boundary leaky dielectric model shows very similar dynamics to the perfect dielectric model, with the exception that the deformation can be negative, or zero. The full leaky dielectric model can show strong effects of the boundary charge dynamics and convective transport of charge along the interface, which can alter the transient response of the droplet to an imposed electric field, as well as the steady state deformation.

The parameters used in the leaky dielectric model are the same as in Table 1, with the addition of a pair of conductivities. These are calculated from Eq. (12), given a set of ion characteristics combined with a temperature and partition coefficient (Eq. 17). The relevant ion characteristics are the absolute concentration in the continuous phase (n_e), valence of

each ion (z^1, z^2), and diffusion coefficient (D_i^1, D_i^2, D_e^1, D_e^2). This allows a fully physical description, as in the perfect dielectric case. This is done in both the static and full leaky dielectric models, even though the static model only requires a conductivity ratio. Table 2 gives the full parameter set. Here, we first describe simulation results using the static boundary condition, Eq. (24) for the leaky-dielectric model. Following this, the simulation results based on the dynamic charge buildup equation, (26), the so-called full leaky dielectric model, will be presented.

5.1 Static Boundary Leaky Dielectric Model

Figure 8 shows the effects of increasing the applied field in the base case. The field is varied from 1 MV/m in the base case to a maximum of 20 MV/m. In Fig. 8(a), the deformations are normalized by the analytical expression for the deformation based on the leaky dielectric model, Eq. (3). In this figure, it can be seen that some of the same effects are present as in the perfect dielectric case, seen in Figure 7. The increase in applied field produces a nonlinear response, accompanied by a decrease in overshoot. However, it is notable that in this case the nonlinearity is in the opposite direction from that observed in the perfect dielectric base case of Figure 7. The high-field deformations are less extreme than predicted by Taylor's result, and all of them have steady-state values. Part of the reason for the reduced deformation at high fields is that the analytic deformation parameter in these cases exceeds -1. This is a physical impossibility, since it requires a negative aspect ratio. The 20 MV/m case has a theoretical deformation parameter of -1.9885 based on Eq. (3), but the numerical result gives only -0.898, which corresponds to an aspect ratio of 0.0539. This may be seen more clearly in Figure 8(b), which is a plot of the data in Figure 8(a) without normalization of the deformation parameter values.

Figure 8(b) shows deformation curves that appear to be asymptotically approaching -1 as the field increases. No instability is apparent, even for severely deformed drops. The reason for this is that the higher fields produce droplets that are essentially squashed into thin disks, with most of the circulation occurring near the outer edge. No points or edges develop that might lead to jet ejection, and the drop does not tend to fragment. This may be seen in Figure 9. In Figure 9, the deformed shapes and circulatory patterns at steady-state are shown. The circulation within the drop, known as a Taylor vortex, can be clearly seen from the vector plots. The stress along the boundary induces tangential flow, which results in a circulatory pattern inside the droplet and an approximately hyperbolic velocity profile outside it. This matches the effect predicted by Taylor [10] and observed by McEwan and de Jong in an addendum to the same paper.

The 10 MV/m case in Figure 9(a) shows a substantial deformation that nevertheless appears approximately spheroidal. The flow pattern is similar to what is seen in lower-deformation cases. The 15 MV/m case, shown in Figure 9(b), has departed entirely from the spheroidal

regime and deformed into a flattened disk shape. The majority of the circulation is occurring near the edge of the disk, and the rest of the droplet is relatively quiescent. The 15 MV/m case is representative of the higher-field cases; the only differences are that for the higher fields, the disk is flatter and the circulation more localized and pronounced. No tendency toward instability or the development of sharp edges is observed. This observation is, however, limited to the specific parameter set studied here. The deformed shape depends on the combination of the viscosity, permittivity, and conductivity ratios of the two fluids.

Figure 10 shows the effect of altering the conductivity ratio with a fixed applied field of 10 MV/m employing the static leaky dielectric model. The conductivity ratio here is equal to the partition coefficient Φ, since none of the ion characteristics vary between the two fluids, and values of Φ between 0.1 and 100 are employed. The case $\Phi = 0.1$ shows a rapid unbounded response which quickly reaches a singular point, beyond which it is not possible to continue the simulation. The next case, $\Phi = 1$, is identical to the 10 MV/m simulation in Figure 8. It shows moderate deformation with a well-defined steady-state. For $\Phi = 10$, the response is very slightly prolate. It should be noted that this value of the partition coefficient is very close to a value of $\Phi = 8.8882$, which corresponds to the case of a non-deformed drop in presence of an applied electric field. In the case where $\Phi = 100$, the deformation is substantially prolate, and has a slightly higher deformation than that predicted by the linear theory.

These results illustrate the alteration that the conductivity ratio can produce in the character of the deformation. The difference between the cases $\Phi = 0.1$ and 1 is particularly striking. Despite the fact that they are both oblate deformations under the same applied field, the $\Phi = 0.1$ case develops a singularity so fast that the simulation is ended before the deformation reaches values as high as the more extreme cases in Fig. 8. The deformation parameter at the singularity in this case is -0.723, which denotes a substantially thicker drop than the value of -0.898 reached by the (stable) 20 MV/m case from Fig. 8.

Figure 11 shows the difference in deformed shape between the $\Phi = 0.1$ case from Figure 10 and two other simulations with $\Phi = 0.2$ and 0.5. The $\Phi = 0.2$ and 0.5 cases in Figure 11 represent steady-states, but the $\Phi = 0.1$ case in Figure 11(a) represents the point at which the boundary becomes singular, as this case has no steady state. The difference in character of the deformation induced by the change in partition coefficient, and hence conductivity ratio, is clear in these figures. The lower ratio of 0.1 causes the drop, under high electric field, to develop a sharp edge around its equator, which constitutes an analogue to the tip streaming mode of breakup. This is also evident from the velocity vector plot in Fig. 11(a). A higher conductivity ratio results in a less extreme shape having no singularities, and a much larger applied field is necessary to produce it.

The conductivity ratios in Fig. 11(b) and (c) are much closer to the crossover point between the sharp-edged and blunt-disk modes of deformation. Figure 11(b) shows a third type of behavior that appears near the transition, in which a toroidal segment pinches off from the main drop. Figure 11(c) shows a case with a larger partition coefficient of 0.5, and it shows

most of the characteristics of the blunt disk droplets. A vestige of the toroidal ring can nevertheless be seen in the widening of this droplet toward its edge.

Transitions between these modes of deformation are here facilitated by changing only a single parameter, the partition coefficient. It is not unlikely that the observed effect is actually part of a compound effect involving the fluid parameters, as well as the permittivity ratio, which is known to affect the character of perfect dielectric deformations [13,27,42].

5.2 Transient Charge Boundary Leaky Dielectric Model

The full leaky dielectric model allows for finite-in-time charge buildup on the interface, as well as steady-state convection effects. This can have a profound effect on the overall response of the droplet to an applied electric field, both in terms of the initial transient and the steady-state deformation.

Figure 12 shows the effect of varying the ionic concentration in the leaky dielectric base case, starting with the static model and demonstrating the effect of lowering the absolute conductivity. In the base case, the conductivities of the two fluids are equal. The dynamic charge simulations were done with monovalent ionic concentrations of 2×10^{-4} M and 4×10^{-5} M, leading to conductivity values of approximately 1.5×10^{-3} S/m and 3×10^{-4} S/m, respectively. The horizontal dashed line indicates the analytic deformation from Taylor's result.

The dynamic response of the static leaky dielectric model is very similar to that of the perfect dielectric model. However, the inclusion of charge dynamics in the form of Eq. (26) increases the complexity of the response significantly. The dynamic boundary cases here show non-minimum-phase behavior; their initial motion is away from the steady-state deformation the droplet will eventually attain. In addition, the lowest-conductivity case shows a significant secondary time scale, slower than the droplet's oscillation frequency, by which relaxation to the final state occurs. The reason for this behavior is the finite charge buildup time. Saville [15] gives the conductive relaxation time constant as ϵ/σ. Initially, the boundary is uncharged, so the dynamic response begins identically to the perfect dielectric case. As the charge builds up, the droplet's deformation changes direction toward the leaky dielectric steady-state limit. If the charge relaxation is significantly slower than the drop oscillation, the transition to steady-state deformation is governed by the charge buildup. This effect is first-order and resembles an exponential, which is shown in the lowest-conductivity case in Figure 12. In an extreme case with very low conductivity, the complete perfect dielectric transient oscillation might occur, followed by a slow, monotonic transition to the leaky dielectric steady-state limit.

Figure 13 shows the complete dynamic response of a leaky dielectric drop using the dynamic

interfacial boundary condition. The parameters are those of the leaky dielectric base case, with an ionic concentration in both fluids of 4×10^{-5} M, leading to a conductivity of 3×10^{-4} S/m. This result demonstrates the effect of charge convection along the drop interface on the steady-state deformation. The steady-state value predicted by Taylor's analytic result, Eq. (3) is shown by the dashed line; clearly, the steady-state value reached by the simulation is different from the analytic prediction. The charge distribution on the interface is modified by the steady-state tangential flows associated with the leaky dielectric system. This effect alters the electrical stress distribution and can modify the steady-state deformation. As noted by Feng [24], the result in the case of oblate deformation is a reduction of the steady-state deformation relative to the analytic result.

6 Comparison With Experiment

Lu [43] reported experiments in which drops of water suspended in organic solvents were subjected to DC electric fields. One of the control tests was a series of measurements of the deformation of a drop of water in decyl alcohol. This experiment was duplicated numerically in this study employing the full leaky dielectric model, and Figure 14 shows the results, where the steady-state deformation of the droplet is plotted against the Weber number, defined as

$$We = \frac{\epsilon_e R_0 E_0^2}{\gamma} \tag{35}$$

The value of the interfacial tension used in the simulations was 0.0089 N/m, as reported in Lu [43].

In Figure 14, the open and solid circles depict two sets of experimental data obtained from [43]. The dashed line represents the steady state deformation predicted using Eq. (3). The open square symbols are the numerical deformation results at steady state, while the solid line is the best fit to the numerical data. For small values of $We < 0.05$, the numerically predicted steady-state deformation seems to be in good agreement with the deformation predicted by Eq. (3). However, at larger values of We, the numerical results seem to indicate a nonlinear increase in deformation with We. A similar trend is observed in the experiments, and the numerical predictions seem to be in good agreement with the experimental data. The nonlinear departure from Taylor's analytic result observed in the numerical simulations for this case is gentle enough that it provides a possible explanation for the observed trend in the experimental data. This also suggests that for large applied fields, the deformation is not proportional to E_0^2, as would be suggested by the linear theory. The agreement between the numerical simulations and experiment seen here is encouraging.

7 Concluding Remarks

Numerical simulations of the transient droplet deformation under the influence of applied electric fields were presented for perfect dielectric and leaky dielectric systems. The finite element moving boundary model developed tracks the droplet deformation in time, and predicts the steady state deformation accurately. Excellent agreement with analytic expressions for steady-state deformations are observed for low applied fields, both for perfect and leaky dielectric systems. The influence of higher applied fields, leading to a non-linear transient response have also be described. For the leaky dielectric system, a wide range of deformed droplet shapes are attainable by simply varying the conductivity, and the conductivity ratio of the two fluids. Finally, the transient charge build up boundary condition, when incorporated in the leaky dielectric model, can show a much slower relaxation of the droplet to a steady-state.

A representative set of results obtained from the numerical simulations, including a comparison with experimental results, indicate that the present model can provide a generalized procedure for assessing droplet deformation under the influence of high applied electric fields. The simulations can easily be extended to other types of electrical forcing, such as oscillating fields, and will allow exploration of a wide range of microscopic droplet dynamics that are being studied in conjunction with electrical de-emulsification or in many microfluidic systems.

Acknowledgments

Financial support for this research from National Sciences and Engineering Research Council of Canada (NSERC) is gratefully acknowledged.

References

[1] A. G. Bailey, Electrostatic spraying of liquids, Wiley: New York, 1988.

[2] J. S. Eow, M. Ghadiri, A. O. Sharif, T. J. Williams, Electrostatic enhancement of coalescence of water droplets in oil: a review of the current understanding, Chem. Eng. J. 84 (2001) 173–192.

[3] J. S. Eow, M. Ghadiri, Motion, deformation and break-up of aqueous drops in oils under high electric field strengths, Chem. Eng. Process. 42 (2003) 259–272.

[4] F. Mostowfi, K. Khristov, J. Czarnecki, J. Masliyah, S. Bhattacharjee, Electric field mediated breakdown of thin liquid films separating microscopic emulsion droplets, Appl. Phys. Lett. 90 (2007) 184102.

[5] H. Moon, S. K. Cho, R. L. Garrell, C. J. Kim, Low voltage electrowetting-on-dielectric, J. Appl. Phys. 92 (7) (2002) 4080–4087.

[6] S. K. Cho, H. J. Moon, C. J. Kim, Creating, transporting, cutting, and merging liquid droplets by electrowetting-based actuation for digital microfluidic circuits, J. Microelectromech. Syst. 12 (1) (2003) 70–80.

[7] B. Shapiro, H. Moon, R. L. Garrell, C. J. Kim, Equilibrium behavior of sessile drops under surface tension, applied external fields, and material variations, J. Appl. Phys. 93 (9) (2003) 5794–5811.

[8] C. T. O'Konski, H. C. Thacher, The distortion of aerosol droplets by an electric field, J. Phys. Chem. 57 (1953) 955–958.

[9] R. S. Allan, S. G. Mason, Particle behaviour in shear and electric fields .1. deformation and burst of fluid drops, Proc. Roy. Soc. Lond. A-Math. Phys. Sci. 267 (1328) (1962) 45–61.

[10] G. I. Taylor, Studies in electrohydrodynamics. i. circulation produced in a drop by an electric field, Proc. Roy. Soc. Lond. A-Math. Phys. Sci. 291 (1425) (1966) 159–166.

[11] J. R. Melcher, G. I. Taylor, Electrohydrodynamics: a review of the role of interfacial shear stresses, Annu. Rev. Fluid Mech. 1 (1969) 111–146.

[12] S. Torza, R. G. Cox, S. G. Mason, Electrohydrodynamic deformation and burst of liquid drops, Phil. Trans. Roy. Soc. Lond. A-Math. Phys. Sci. 269 (1198) (1971) 295–319.

[13] J. D. Sherwood, Breakup of fluid droplets in electric and magnetic-fields, J. Fluid Mech. 188 (1988) 133–146.

[14] J. C. Baygents, D. A. Saville, The circulation produced in a drop by an electric field: a high field strength electrokinetic model, in: T. G. Wang (Ed.), Drops and Bubbles: Third Intl. Colloq., American Institute of Physics, 1989, pp. 7–17.

[15] D. A. Saville, Electrohydrodynamics: the taylor-melcher leaky dielectric model, Annu. Rev. Fluid Mech. 29 (1997) 27–64.

[16] E. K. Zholkovskij, J. H. Masliyah, J. Czarnecki, An electrokinetic model of drop deformation in an electric field, J. Fluid Mech. 472 (2002) 1–27.

[17] N. Bentenitis, S. Krause, Droplet deformation in dc electric fields: the extended leaky dielectric model, Langmuir 21 (2005) 6194–6209.

[18] J. Q. Feng, K. V. Beard, Small-amplitude oscillations of electrostatically levitated drops, Proc. Roy. Soc. Lond. A-Math. Phys. Sci. 430 (1878) (1990) 133–150.

[19] J. Q. Feng, K. V. Beard, Resonances of a conducting drop in an alternating electric field, J. Fluid Mech. 222 (1991) 417–435.

[20] J. Q. Feng, K. V. Beard, 3-dimensional oscillation characteristics of electrostatically deformed drops, Proc. Roy. Soc. Lond. A-Math. Phys. Sci. 227 (1991) 429–447.

[21] J. W. Ha, S. M. Yang, Effects of surfactant on the deformation and stability of a drop in a viscous-fluid in an electric-field, J. Colloid Interf. Sci. 175 (2) (1995) 369–385.

[22] J. Q. Feng, T. C. Scott, A computational analysis of electrohydrodynamics of a leaky dielectric drop in an electric field, J. Fluid Mech. 311 (1996) 289–326.

[23] J. W. Ha, S. M. Yang, Effect of nonionic surfactant on the deformation and breakup of a drop in an electric field, J. Colloid Interf. Sci. 206 (1998) 195–204.

[24] J. Q. Feng, Electrohydrodynamic behaviour of a drop subjected to a steady uniform electric field at finite electric reynolds number, Proc. Roy. Soc. Lond. A-Math. Phys. Eng. Sci. 455 (1986) (1999) 2245–2269.

[25] P. R. Brazier-Smith, Stability and shape of isolated and pairs of water drops in an electric field, Phys. Fluids 14 (1) (1971) 1–6.

[26] P. R. Brazier-Smith, S. G. Jennings, J. Latham, An investigation of the behaviour of drops and drop-pairs subjected to strong electrical forces, Proc. Roy. Soc. Lond. A-Math. Phys. Sci. 325 (1562) (1971) 363–376.

[27] M. J. Miksis, Shape of a drop in an electric field, Phys. Fluids 24 (11) (1981) 1967–1972.

[28] O. A. Basaran, L. E. Scriven, Axisymmetric shapes and stability of charged drops in an external electric field, Phys. Fluids A 1 (5) (1989) 799–809.

[29] O. A. Basaran, T. W. Patzek, R. E. Benner, L. E. Scriven, Nonlinear oscillations and breakup of conducting, inviscid drops in an externally applied electric field, Ind. Eng. Chem. Res. 34 (10) (1995) 3454–3465.

[30] R. J. Haywood, M. Renksizbulut, G. D. Raithby, Transient deformation of freely-suspended liquid droplets in electrostatic fields, AICHE Journal 37 (9) (1991) 1305–1317.

[31] T. Tsukada, T. Katayama, Y. Ito, M. Hozawa, Theoretical and experimental studies of circulation inside and outside a deformed drop under a uniform electric field, J. Chem. Eng. Japan 26 (1993) 698–703.

[32] T. Hirata, T. Kikuchi, T. Tsukada, M. Hozawa, Finite element analysis of electrohydrodynamic time-dependent deformation of dielectric drop under uniform dc electric field, J. Chem. Eng. Jpn. 33 (1) (2000) 160–167.

[33] O. A. Basaran, Nonlinear oscillations of viscous liquid drops, J. Fluid Mech. 241 (1992) 169–198.

[34] J. H. Masliyah, S. Bhattacharjee, Electrokinetic and Colloid Transport Phenomena, Wiley Interscience, New Jersey, 2006.

[35] COMSOL, FEMLAB Reference Manual, COMSOL AB, version 2.3 (2002).

[36] D. L. Whitaker, C. Kim, C. L. Vicente, M. A. Weilert, H. J. Maris, G. M. Seidel, Shape oscillations in levitated he ii drops, J. Low Temp. Phys. 113 (1998) 491–499.

[37] G. Supeene, Numerical simulation of time-dependent droplet deformation in an electric field, Master's thesis, University of Alberta (Canada) (2006).

[38] P. N. Brown, A. C. Hindmarsh, L. R. Petzold, Using krylov methods in the solution of large-scale differential-algebraic systems, SIAM J. Sci. Comput. 15 (1994) 1467–1488.

[39] P. N. Brown, A. C. Hindmarsh, L. R. Petzold, Consistent initial condition calculation for differential-algebraic systems, SIAM J. Sci. Comput. 19 (1998) 1495–1512.

[40] G. M. Supeene, C. R. Koch, S. Bhattacharjee, Deformation of a droplet in an electrical field: Transient response in dielectric media, J. Comp. Theor. Nanosci. 1 (4) (2004) 429–437.

[41] C. G. Garton, Z. Krasucki, Bubbles in insulating liquids: stability in an electric field, Proc. Roy. Soc. Lond. A-Math. Phys. Sci. 280 (1381) (1964) 211–226.

[42] C. E. Rosenkilde, A dielectric fluid drop in an electric field, Proc. Roy. Soc. Lond. A-Math. Phys. Sci. 312 (1511) (1969) 473–494.

[43] Y. Lu, Electrohydrodynamic deformation of water drops in oil with an electric field, Master's thesis, University of Alberta (Canada) (2002).

Table 1
Simulation parameters for the perfect dielectric base case.

Applied Electric Field E_0	1 MV/m
Droplet Radius R_0	1 μm
Droplet Relative Permittivity ϵ_i	80
Medium Relative Permittivity ϵ_e	3
Interfacial Tension γ	0.03 N/m
Droplet Density ρ_i	1000 kg/m^3
Medium Density ρ_e	1000 kg/m^3
Droplet Viscosity μ_i	0.001 Pa·s
Medium Viscosity μ_e	0.001 Pa·s

Table 2
Simulation parameters for the leaky dielectric base case

Applied Electric Field E_0	1 MV/m
Droplet Radius R_0	1 μm
Droplet Relative Permittivity ϵ_i	80
Medium Relative Permittivity ϵ_e	3
Interfacial Tension γ	0.03 N/m
Droplet Density ρ_i	1000 kg/m^3
Medium Density ρ_e	1000 kg/m^3
Droplet Viscosity μ_i	0.001 Pa·s
Medium Viscosity μ_e	0.001 Pa·s
Medium Ionic Concentration c_e	0.04 mol/m^3 (4×10^{-4} M)
Ion Partition Coefficient (i/e) α	1.0
Positive Ion Valence z^1	1
Negative Ion Valence z^2	-1
Droplet +ve Ion Diffusion Coefficient D_i^1	10^{-9} m^2/s
Droplet $-$ve Ion Diffusion Coefficient D_i^2	10^{-9} m^2/s
Medium +ve Ion Diffusion Coefficient D_e^1	10^{-9} m^2/s
Medium $-$ve Ion Diffusion Coefficient D_e^2	10^{-9} m^2/s
System Temperature T	298 K

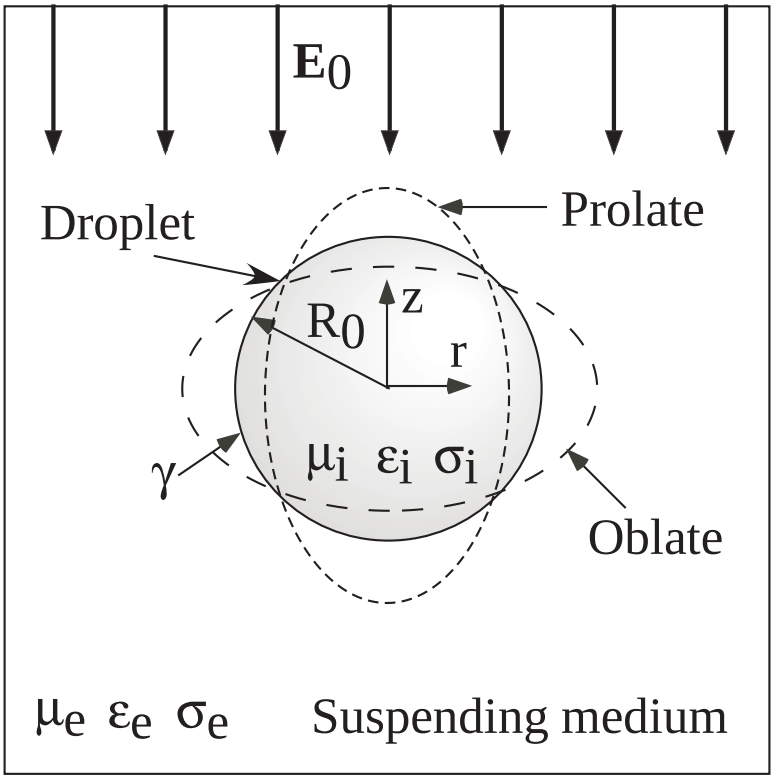

Fig. 1. Schematic representation of the deformation of a droplet suspended in a second fluid in the presence of an electric field, $\mathbf{E}_0$, acting along the z axis of the cylindrical coordinate system. The shaded circle represents the spherical non-deformed droplet before application of the field. The possible steady-state deformed shapes, prolate and oblate spheroids, are also depicted. The non-deformed droplet diameter is R_0. The relevant properties of the droplet and suspending medium are the viscosity, μ, dielectric permittivity, ϵ, and conductivity, σ. The subscripts i and e are used to represent the droplet and the suspending fluid, respectively. The interfacial tension, γ, constitutes the restoring force.

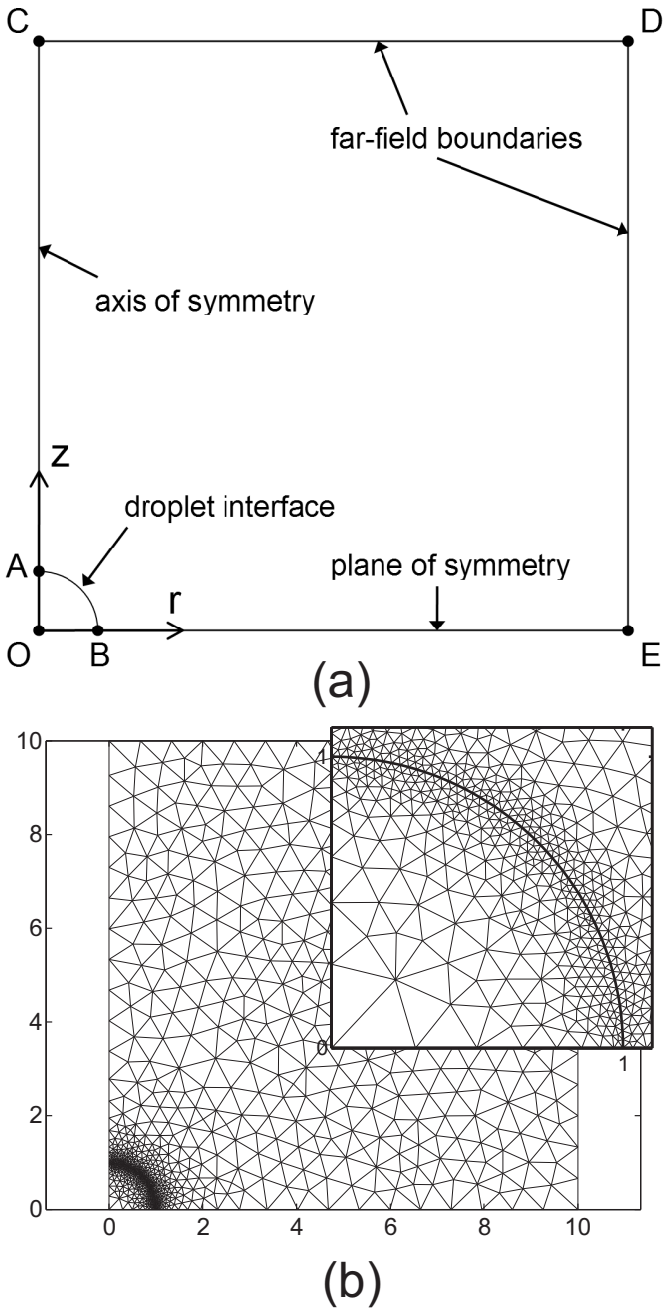

Fig. 2. (a) Two-dimensional axisymmetric geometry for the numerical solution. (b) Typical meshed geometry. Dimensions are scaled with respect to the drop radius. The inset shows the details of the mesh near the droplet boundary.

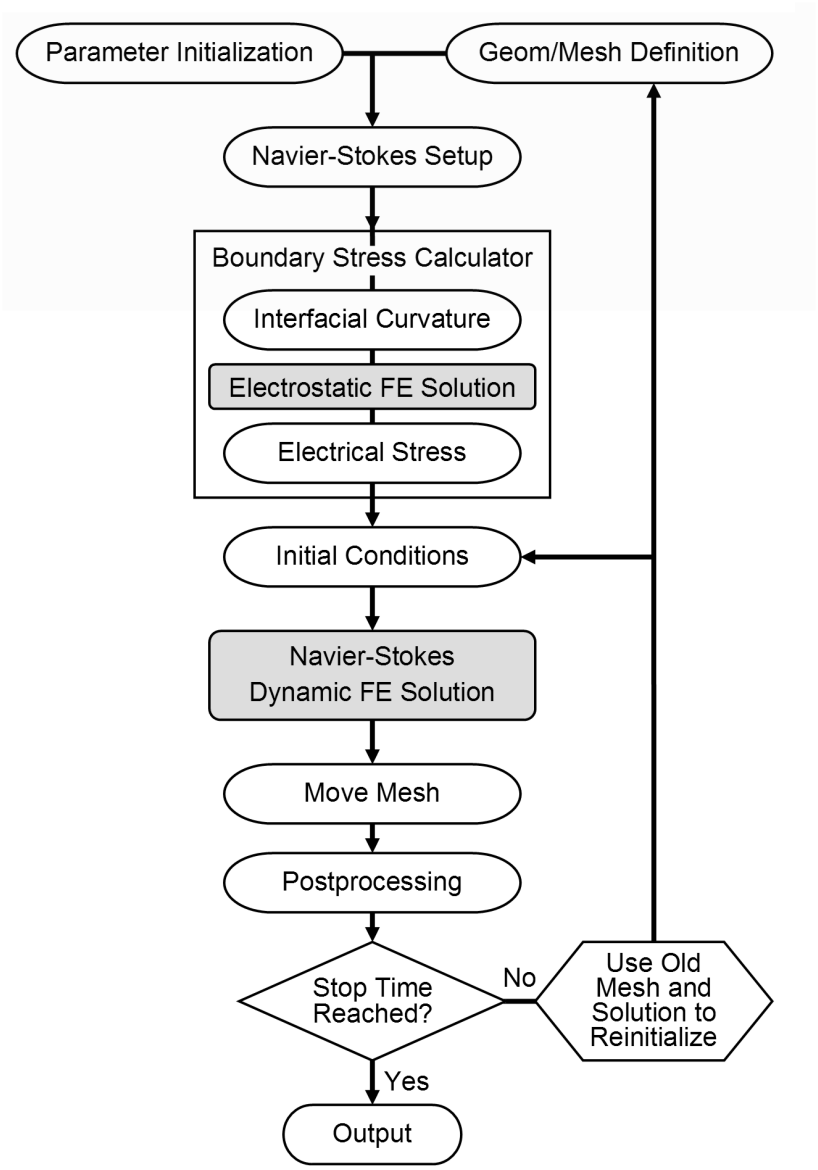

Fig. 3. Structure of the dynamic finite element solution.

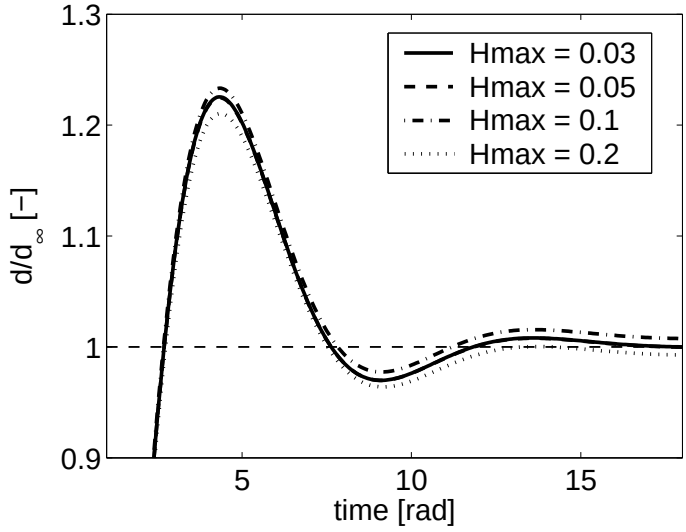

Fig. 4. Variation of dynamic response for increasing mesh refinement at drop interface. The parameter varied is mesh size specification in the finite element code, applied here to the interfacial boundary only. The non-dimensional time step is 0.06.

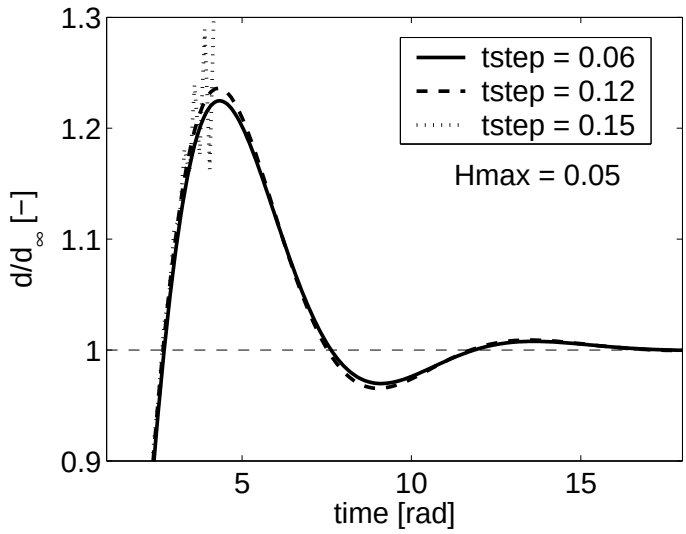

Fig. 5. Convergence of dynamic response with time step, for a 33-node interface.

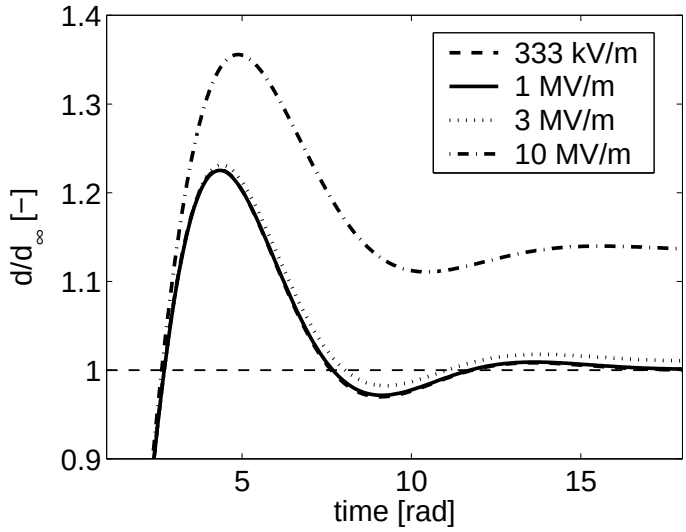

Fig. 6. Normalized dynamic responses for variation in electric fields: Perfect dielectric model.

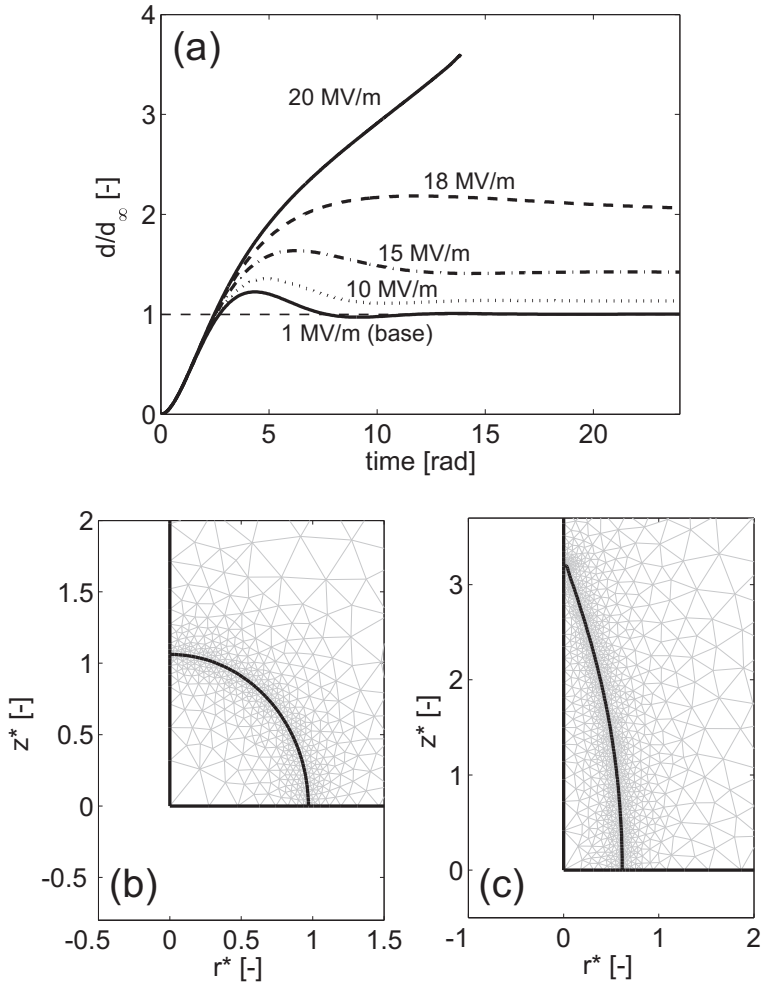

Fig. 7. (a) Normalized dynamic responses for high applied fields, using the perfect dielectric model. (b) and (c): Deformed droplet shape at end of run for an applied field of 10 MV/m and 20 MV/m, respectively.

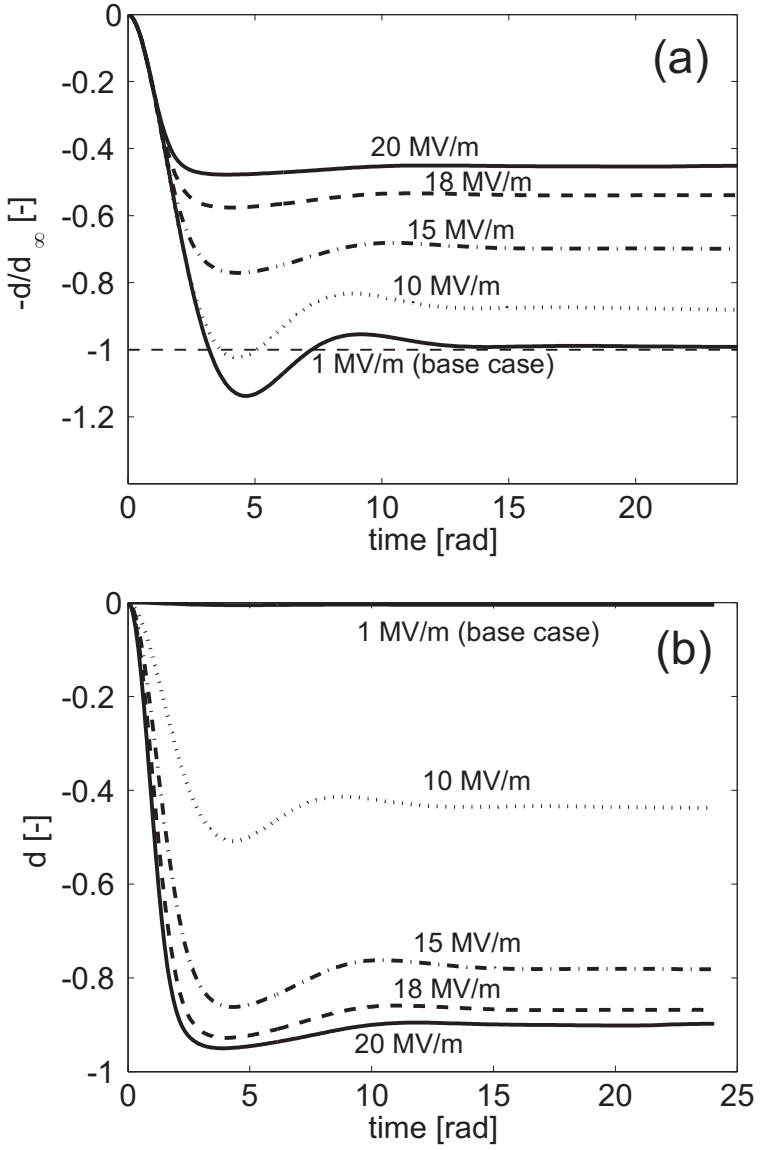

Fig. 8. Effect of high applied fields on the static leaky dielectric response. (a) deformations scaled with respect to the Taylor expression for the steady-state deformation, d_∞, given by Eq. (3). (b) Actual variation of the deformation parameter with scaled time.

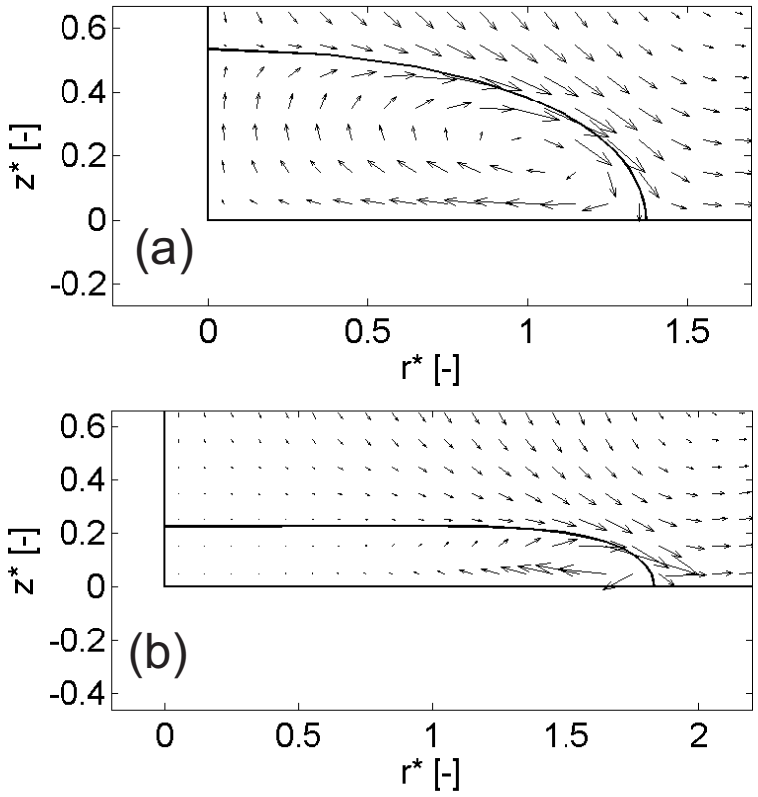

Fig. 9. Deformed steady-state droplet shape and velocity field at end of the static leaky-dielectric simulations for (a) 10 MV/m and (b) 15 MV/m. Steady-state fluid circulation is depicted by the vector plots in either case.

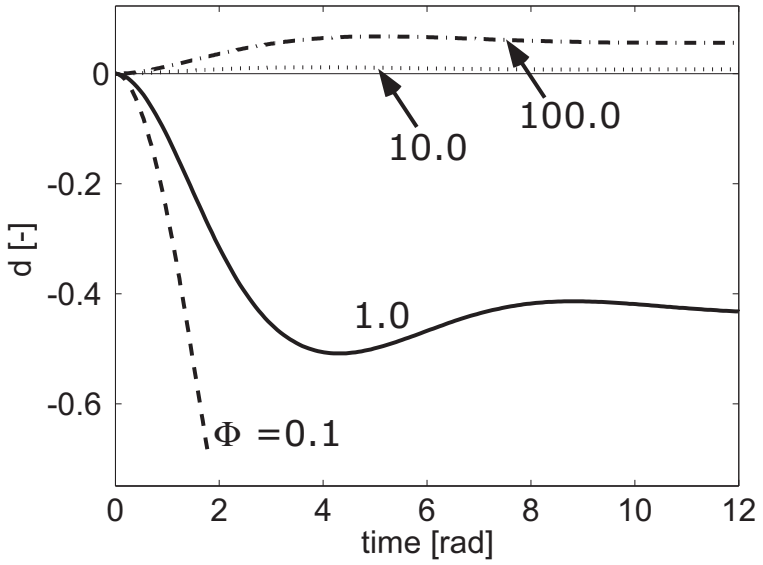

Fig. 10. Effect of conductivity ratio on the character of the nonlinearity for an applied field of 10 MV/m.

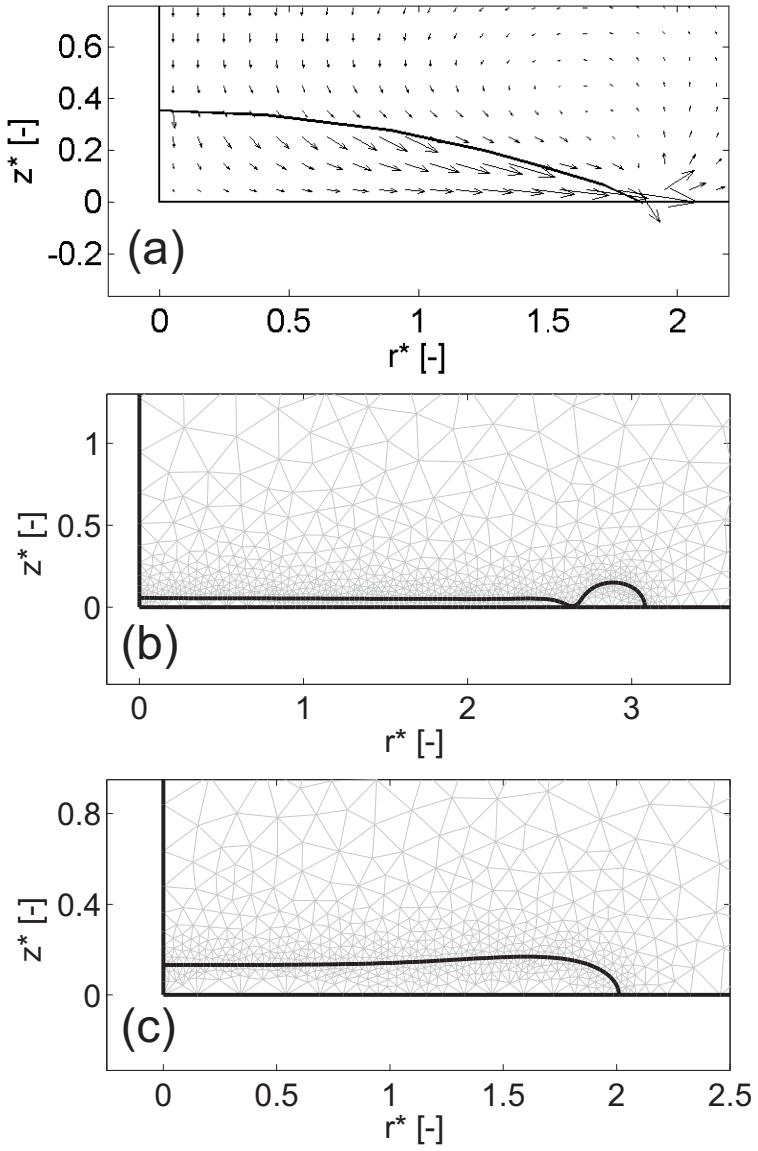

Fig. 11. Deformed droplet shape at end of run, for (a) $\Phi = 0.1$, (b) $\Phi = 0.2$ and (c) $\Phi = 0.5$, all obtained for an applied field of 10 MV/m.

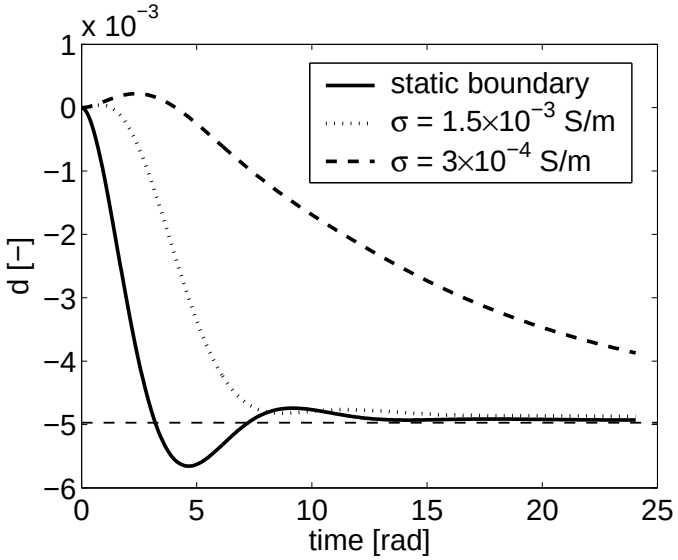

Fig. 12. Dynamic contribution from charge relaxation on interface for various fluid conductivities in the full leaky dielectric model.

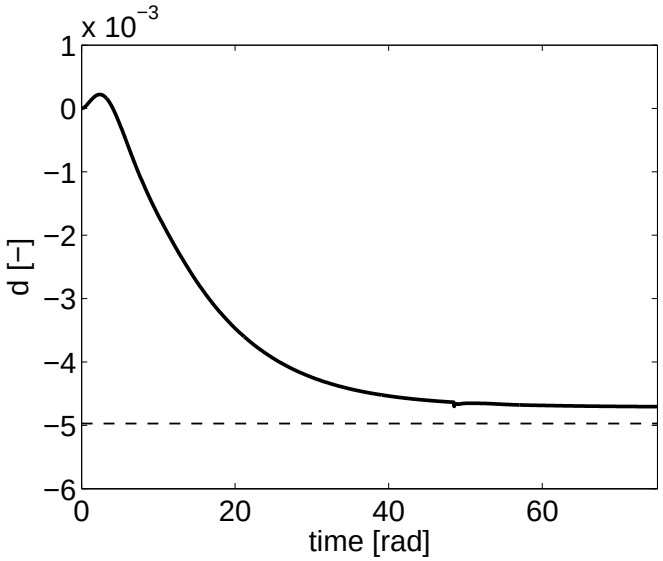

Fig. 13. Steady-state offset from Taylor limit resulting from charge convection in the full leaky dielectric model.

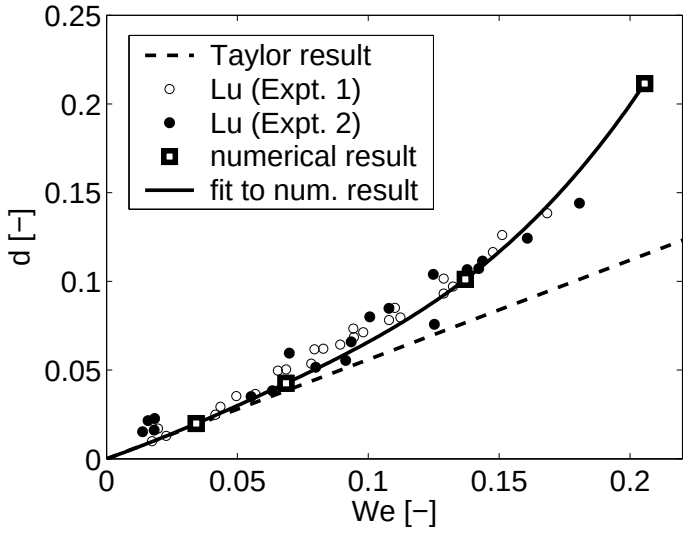

Fig. 14. Steady-state deformation parameter plotted against Weber number for water in decyl alcohol: Comparison of numerical simulations with experimental data [43] and analytic steady-state deformation based on Taylor model.